López de Armentia, S., Pantoja, M., Abenojar, J., Martínez, M.A. (2018). Development of Silane-Based Coatings with Zirconia Nanoparticles Combining Wetting, Tribological, and Aesthetical Properties. *Coatings*, 8 (10), 368.

DOI: https://doi.org/10.3390/coatings8100368

coatings

MDPI

Article

Development of Silane-Based Coatings with Zirconia Nanoparticles Combining Wetting, Tribological, and Aesthetical Properties

Sara Lopez de Armentia, Mariola Pantoja, Juana Abenojar * and Miguel Angel Martinez

Department of Materials Science and Engineering (IAAB), Universidad Carlos III of Madrid, Av. Universidad 30, 28911 Leganés, Spain; slopezar@pa.uc3m.es (S.L.d.A.); mpruiz@ing.uc3m.es (M.P.); mamc@ing.uc3m.es (M.A.M.)

* Correspondence: abenojar@ing.uc3m.es; Tel.: +34-91-624-8863

Received: 24 September 2018; Accepted: 15 October 2018; Published: 18 October 2018

Abstract: Silane-based coatings with nanoparticles have been widely used in applications related to surface protection. Between them, the improvement of corrosion resistance by increasing the hydrophobicity is one of the main research goals. However, most coatings present problems of low wear resistance and poor aesthetic appearance. Therefore, the overall goal of this research is to manufacture hydrophobic sol-gel coatings based on silanes which comply with good tribological and aesthetical properties. In the present study, stainless steel plates were coated with a silane-based solution containing zirconia nanoparticles by dip coating. Water–ethanol solutions with silanes (methyltrimethoxysilane (MTS) and tetrathoxysilane (TEOS)) and different percentages of ZrO_2 nanoparticles were prepared. Gloss, color, contact angle, surface energy, wear resistance, and thickness of coating were analyzed to elucidate the effect of zirconium oxide on the performance of the coatings. Results demonstrate that the ZrO_2–silane coatings on stainless steel offer a balanced combination of properties: low wettability, high wear resistance, and similar color and brightness compared to pristine stainless steel.

Keywords: sol-gel; silanes; ZrO_2; wear resistance; gloss; color

1. Introduction

Inorganic sol-gel coatings based on metal/oxygen networks are widely used for protecting metals such as stainless steel, aluminum, and copper from oxidation and corrosion. These kinds of coatings promote high corrosion resistance, but interfacial adhesion, shrinkage, and oxidation of the substrate remain a problem. To avoid these problems, organic–inorganic hybrid coatings are investigated. Besides, organic–inorganic coatings have been found to impart more hydrophobic character than the inorganic, which improves corrosion resistance [1].

Nowadays, silane-based organic coatings are highly used due to the enhancement of surface-related properties of some materials. The most extended applications of these coatings are associated with the isolation and protection in corrosive environments [2,3], surfaces with hydrophobic properties [4,5], and improvement of adhesive characteristics [6,7]. Other applications are focused on the flame-retardant effect of hybrid organic–inorganic coatings [8]. Good wear resistance is required for most of these applications. However, the most commonly used coatings are based on materials with poor tribological properties.

Several reports concerning the use of nanoparticles and silanes study how they modify different properties of coatings, ranging from chemical, wear, and corrosion resistance to the antibacterial and photocatalytic activity. For instance, previous studies [9–12] have shown that the addition of ceramic

nanoparticles in the coatings enhances significantly the durability of these coatings, and the puncture force. Benerjee et al. [13] developed silica nanoparticle-reinforced fluorinated coatings on glass by dip coating in order to increase hardness, wear resistance, and hydrophobicity of surfaces.

Zirconium oxide (ZrO_2) nanoparticles have shown excellent properties such as strength, fracture toughness, wear resistance, chemical resistance, and hardness [14]. ZrO_2 nanoparticles have been researched as corrosion inhibitor in sol-gel coatings, enhancing the corrosion resistance of metallic substrates [15,16]. Some works [17,18] show that the addition of ZrO_2 nanoparticles improves thermal resistance as well as corrosion resistance. ZrO_2 nanofilms made by atomic layer deposition on magnesium substrate also show an improvement on corrosion resistance [19].

There are some studies about tribological properties of coatings with zirconia [20,21]. Yen et al. [22] observed less wear loss and lower friction coefficient of Co-Cr-Mo alloy specimens thanks to the electrolytic deposition of ZrO_2. However, studies about wear resistance and the aesthetic appearance of silane-based coatings with zirconia nanoparticles, as it has been mentioned previously, could not be found in literature. Therefore, the aim of the present work is to manufacture sol-gel coatings meeting low wettability, high wear resistance and transparence using an economic and easy method. Hence, tribological properties, aesthetic appearance, wettability and coating thickness are studied in this research. In order to achieve it, different percentages of zirconia nanoparticles have been added to silane solutions which have been used to coat stainless steel plates.

This coating is designed for habitat industry according to Sudoe Project, which funds this work. It could be applied on steel of kitchen (countertops, extractor hoods or appliances) or bathroom (countertops). Nowadays, metals are used in interior and exterior design by architects and designers, where this type of transparent coating with low wettability and wear resistance would be very useful.

2. Experimental

2.1. Materials and Preparation of Coatings

Silanes used to manufacture the coatings were tetraethoxysilane (TEOS) and methyltrimethoxysilane (MTS), both supplied by ABCR GmbH & Co. KG (Karlsruhe, Germany). They were mixed with a mixture of water and ethanol in molar proportion 1:1, and adjusted to pH 4 with 0.1 M acetic acid. The molar ratio of the final solution corresponded to the formula $(T_1M_2)_1E_3W_3$, where T = TEOS, M = MTS, E = ethanol, W = water. Both silanes were used in a previous research [23].

ZrO_2 nanoparticles were supplied by M K Impex Corp., Mississauga, ON, Canada. They were 99.99% purity and their size was 45 nm, although they are normally bonded together, as Figure 1 shows, where agglomerations of about 0.5 and 1 μm are found, formed by smaller particles. Different amounts of ZrO_2 (1 wt.%, 2.5 wt.% and 5 wt.%) were added to the solution and this final mixture was stirred for 15 min and hydrolyzed for 24 h.

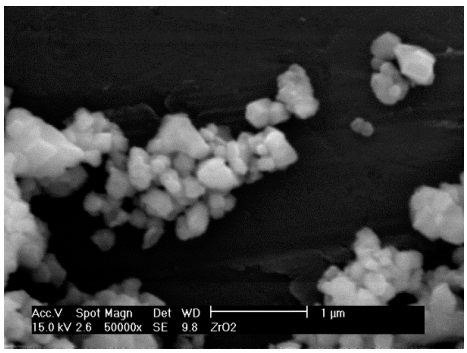

Figure 1. As received ZrO_2 nanoparticles.

The substrate used for coating was an austenitic stainless steel (EN 1.4301). This steel was cut in rectangular plates of 6 × 2 cm^2. The stainless steel plates were coated with the nanoparticle–silane

solution by dip coating. Withdrawal speed used was 400 mm/min and immersion time was 1 min. Then, plates were dried at 110 °C for 1 h.

2.2. Silane Solution Characterization

2.2.1. Surface Tension

Surface tension of solutions used for coatings was measured in order to determine their wettability on the stainless steel. Pendant drop method was used to determine it, employing a goniometer OCA 15 plus (Dataphysics, Neurtek Instruments, Éibar, Spain). Surface tension of silane solutions was measured after they were hydrolyzed (for 24 h).

Drops were formed in two different environments: air and cyclohexane. Thus, it was possible to calculate polar and dispersive components of surface tension with SCA20 software (version 1.0).

2.2.2. Fourier Transform Infrared Spectroscopy

A Brucker Tensor 27 spectrometer from Brucker Optik GmbH (Ettlingen, Germany) equipped with a Golden Gate ATR accessory from Specac (Orpington, UK) was used to obtain the infrared spectra of pristine reagents (pure silanes, solvent (EtOH/H_2O) and nanoparticles) as well as silane solutions containing ZrO_2 nanoparticles. Measurements were carried out with attenuated total multiple reflection technique (ATR). The ATR-IR spectra were recorded taking 100 scans with a resolution of 4 cm^{-1} and wavenumber ranging from 4000 to 650 cm^{-1}. The background corresponded to a spectrum obtained by using the equipment without any sample.

2.2.3. Dynamic Light Scattering

Dynamic light scattering (DLS) using Zetasizer Nano-ZS, Malvern Instruments (Worcestershire, UK) was used to determine the size of agglomerates in the silane solution as a function of the percentage of nanoparticles. DLS measurements were carried out in the solutions with 1 wt.%, 2.5 wt.%, and 5 wt.% of zirconia. These measurements were recorded 24 h after the preparation of the solution and after stirring for, at least, 15 min.

2.3. Surface Characterization

2.3.1. X-ray Fluorescence

A Spectro Xepos energy dispersive X-ray fluorescence (XRF) spectrometer (Spectro Analytical Instruments, Kleve, Germany) with a palladium anode of 50 W was used to qualitatively determine the composition of coatings, measuring Si and Zr percentages. These measurements were made on the coated plates. This spectrometer was provided by Ametek Materials Analysis Division (Kleve, Germany).

2.3.2. Coating Thickness

To measure coating thickness, scratch tester Elcometer 3000 (Rochester Hills, MI, USA) and roughness tester (Hommelwerke GmbH, Villingen-Schwenningen, Germany) were used. It was possible to estimate the thickness with the roughness profile of the plates with a scratch that pierced the coating. For that, scratches with different loads were performed until the device detected contact with metal.

Furthermore, Olympus DSX500 opto-digital microscope (Olympus Industrial, Essex, UK) allow checking the value of the coating thickness measured by scratch.

2.3.3. Fourier Transform Infrared Spectroscopy

Coated surfaces were analyzed by IR spectroscopy with the same spectrometer (Brucker Optik GmbH (Ettlingen, Germany), using the reflection-absorption infrared reflectance spectroscopy (RAIR)

technique. The spectra were recorded with a resolution of 4 cm^{-1} from 4000 to 400 cm^{-1}, taking 128 scans at an angle of 80°. A stainless steel sample without coating was used as a background.

2.3.4. Scanning Electron Microscopy

In order to confirm the presence of ZrO_2 agglomerates on the surfaces, scanning electron microscopy (SEM) equipment (Philips XL-30 SEM, Eindhoven, The Netherlands) was used, coupled with an energy dispersive X-ray spectrometry (EDS) semiquantitative analyzer. The samples were analyzed after gold sputtered coating with Polaron SC7610 (VG Microtech, Uckfield, UK).

2.3.5. Color and Gloss

CIELAB system measures color in a three-dimensional space, defined by the coordinates "L^*", "a^*", and "b^*". The first one corresponds to luminosity: 0 is black and 100 is white; coordinate "a^*" measures variation between red ($+a^*$) and green ($-a^*$); and "b^*" gives changes between yellow ($+b^*$) and blue ($-b^*$). Aesthetical appearance was characterized using color and specular gloss measurements, as it is required by architects and designers. $L^*a^*b^*$ coordinates were measured with a ColorEye XTH portable colorimeter, (X-Rite Pantone®, Grand Rapids, MI, USA).

Finally, variation of color (ΔE) was calculated (Equation (1)) in order to measure the module of the vector from the reference to the measurement. As a color reference, plates without coating were selected. ΔE values lower than 10 are considered acceptable as it was assumed in previous works [24,25].

$$\Delta E = (\Delta L^{*2} + \Delta a^{*2} + \Delta b^{*2})^{1/2} \quad (1)$$

Specular gloss was measured using a Dr. Lange, REFO 3 reflectometer (Düsseldorf, Germany) equipment, with an angle of 85°. At least three measurements were carried out for each coating.

2.3.6. Contact Angle

Hydrophobicity was determined by water static contact angle measurements. OCA 15 Plus from DataPhysics (Neurtek Instruments, Eibar, Spain) goniometer was used for doing these measurements and contact angles were determined using sessile drop method with the SCA20 software. The volume of the drops were 3 μL, and at least ten drops were measured for each sample.

2.3.7. Wear Resistance

The tribological tests were conducted at room temperature and 30% relative humidity (RH) with a pin-on-disk tribometer TDP/10/SCM (Microtest, Madrid, Spain). This device was equipped with a flat circle of P1000 sandpaper that wore the surface. This test directly provides the coefficient of friction as a function of the sliding distance or, in this case, number of cycles.

The parameters selected for the test were a normal load of 5 N and 100 cycles at a sliding speed of 60 rpm. The coatings were able to endure this test were subjected to another test with a normal load of 10 N at 60 rpm and the necessary cycles to produce the failure of the coatings. Three tests were carried out for each surface.

3. Results

3.1. Characterization of Solutions

Using pendant drop method [26], surface tension of ethanol/water and its mix with silanes were calculated. The surface tension values are shown in Table 1, not finding meaningful differences between the solutions without nanoparticles. The most relevant finding is related to the polar and dispersive components. An increase in the polar fraction is observed for silane-solvent solution. This can be understood by taking into account that water molecules present in solution hydrolyze silane molecules, appearing silanol groups (SiOH).

Table 1. Surface tension (σ_T), polar (σ_P), and dispersive (σ_D) components of the ethanol/water (EW) and its combinations with silanes and ZrO_2.

Solution	σ_T (mN/m)	σ_P (mN/m)	σ_D (mN/m)
EW	27.7 ± 0.3	9.9 ± 0.1 (36%)	17.8 ± 0.4 (64%)
Silane–EW	24.1 ± 2.9	19.0 ± 3 (79%)	5.1 ± 1.6 (21%)
Silane–EW + 1 wt.% ZrO_2	32.1 ± 0.9	6.5 ± 1.4 (20%)	25.6 ± 1 (80%)
Silane–EW + 2.5 wt.% ZrO_2	32.8 ± 0.8	12.9 ± 1.7 (39%)	19.9 ± 1.5 (61%)
Silane–EW + 5 wt.% ZrO_2	32.3 ± 0.2	7.4 ± 0.3 (23%)	24.9 ± 0.3 (77%)

Note: Percentage of polar and dispersive contributions indicated in parentheses.

Surface tension increases when ZrO_2 nanoparticles are added into silane solution, finding similar values for the different ZrO_2 amounts. The most important feature is the dramatic increase of dispersive fraction when ZrO_2 nanoparticles are present in the solution. For silane solution, 79% of the surface tension value is due to its polar characteristics, while it is only 20%–39% in silane–ZrO_2 solutions. Several researches [27–29] inform that the ZrO_2 powder dispersed in water can easily adsorb H^+ and OH^- ions on its surface and form a hydration layer. This layer could be related to the disappearance of a portion of SiOH groups in the solution in presence of ZrO_2, even they may form SiOSi siloxane bonds, with dispersive character [30], by reacting with each other. It could also be explained by the bonding between these charged ZrO_2 nanoparticles with the water molecules, by hydrogen bonds, which also affects the polarity of the solution.

Total surface energy of the stainless steel substrate is 51.45 mN/m, higher than the surface tension of all silane solutions. This implies that all silane solutions will wet the substrate properly [31]. Furthermore, the contact angle of the silane and silane–ZrO_2 solutions on stainless steel were measured, obtaining values lower than 10°.

To determine the species in the solutions, ATR-FTIR technique was used. Figure 2 shows the normalized FTIR spectra of ZrO_2 nanoparticles (1 wt.%) in EtOH/H_2O (Figure 2a) and silane solution ($(T_1M_2)_1E_3W_3$) (Figure 2b).

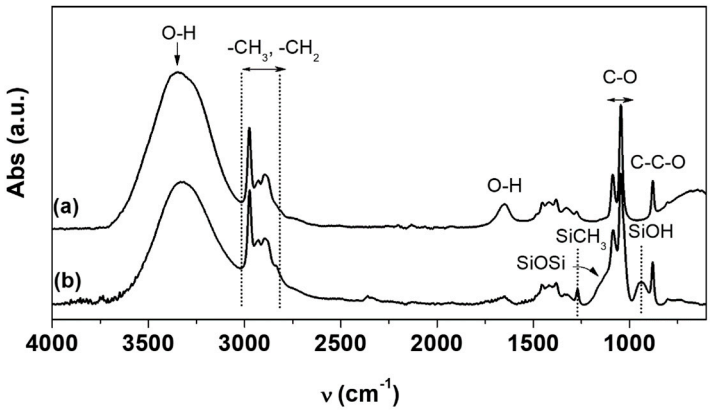

Figure 2. FTIR-ATR spectra of (**a**) EtOH/H_2O with ZrO_2 and (**b**) silane solution ($(T_1M_2)_1E_3W_3$).

Peaks around 3327 cm^{-1} correspond to freely vibrating OH groups and hydrogen bonded OH groups. Bands at 2972 cm^{-1} show the presence of C–H bonds, from ethanol and the bands at 1085 and 1050 cm^{-1}, which are related to C–O bonds [32].

The bands due to alcoxy groups (methoxy, SiOMe, and ethoxy, SiOEt) [33–35] overlap in the same region than the E-W solvent bands (C–O) [36], as shown in Figure 2. Therefore, following the hydrolysis process is not possible from the disappearance of these bands. However, the band related to silanol groups (SiOH) [37], lying around 920 cm^{-1} (Figure 2b), affirmed that the hydrolysis process had taken place. Moreover, the presence of this band, corresponding to silanol specimens, explained the observed increase in the polar fraction when the silanes are in solution (Table 1). The condensation process occurs due to the reaction between silanol groups, according to the reactions described in previous

works [20]. The bands related to these groups appear in 1190–1000 cm^{-1} region, also overlapping with C–O vibration modes of EtOH/H_2O. Silane–ZrO_2 spectrum (Figure 2b) shows that these signals (at 1085 and 1050 cm^{-1}) have a shoulder shifted to high wavenumber (around 1160 cm^{-1}) due to siloxane bonds.

Regarding to the silanol (Si–OH) bands in FTIR spectra of the coatings, it is needed to have a large number of SiOH groups in the solution for getting a good adhesion with the substrate, as it is demonstrated in previous works [6]. In this way, hydrolysis time and pH were optimized to the values used in this work (1 h and pH 4).

Several studies [38,39] assign the bands at 3780–3660 and 1560 cm^{-1} to the absorption bands of ZrOH and Zr–H vibrations. These bands cannot be assigned because both of them appear slapped with the bands of solvent.

According to the supplier, the mean raw ZrO_2 particle size is 45 nm. DLS measurements can determine the agglomeration degree of these nanoparticles in the solvent (ethanol–water) and its ability to disperse them. Results of number size distributions are displayed in Figure 3, for the different percentages of ZrO_2. Particles with size much higher than 45 nm are found. It indicates the occurrence of agglomeration when the particles are in the solvent. A bimodal distribution is observed for the solution with 1 wt.% of ZrO_2, where two predominant particle sizes are observed, around at 1260 and 4780 nm. The distribution only has one peak for 2.5 wt.% and 5 wt.% ZrO_2, centered at 3200 and 1500 nm, respectively.

The differences on agglomeration sizes are explained by the equilibrium between attractive and repulsive forces between the nanoparticles, which present a dipolar moment due to the differences of electronegativity of the elements that form them. The highest attractive forces are found for 2.5 wt.% ZrO_2, being the repulsive forces increased for a higher percentage. It can be considered that the system works as ions (in this case dipoles) in an ionic bond.

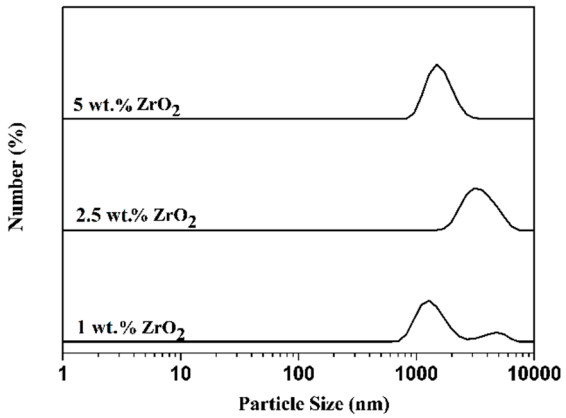

Figure 3. Distribution of particle size for ZrO_2-silane solution at the different percentages of nanoparticles (1 wt.%, 2.5 wt.%, and 5 wt.%) by DLS.

Tang et al. [28] measured the particle size of ZrO_2 nanoparticles in aqueous solution at different pH conditions, indicating that ZrO_2 nanoparticles agglomeration is due to ZrO_2 surface charging as a consequence of adsorption of ions on its surface. They suggested that these charged nanoparticles can easily agglomerate by formation of interactions (hydrogen bonds or van der Waals attractions) with each other. This explains that the particle size found is larger than that supposed from supplied powder (45 nm) due to agglomeration, and it should provide an understanding of why the polar contribution at surface tension for silane solution decreases in presence of ZrO_2 nanoparticles.

3.2. Characterization of Coatings

XRF results are summarized in Table 2. The presence of silane coating and ZrO_2 nanoparticles is verified from the silicon and zirconium percentages measured, respectively. It is observed that the amount of silane on the substrate increases when there is zirconia in the coatings. Silicon percentages higher than 18% are measured for ZrO_2–silane coatings, while lower than 15% are found for the coating without ZrO_2. This is coherent with the surface tension and DLS results argued above. If interactions are established between SiOH groups with each other and/or with ZrO_2, the amount of silane–ZrO_2 solution on metallic substrate should be higher too, explaining the XRF results observed in Table 2. These results are directly related to coating thickness since the penetration depth of XRF is higher than it. To validate this theory, coating thickness was estimated using scratch and roughness measurements and using the optical profilometer (Table 2). Silane coating thickness (0 wt.% ZrO_2) could not be measured as it was too thin. Results show that the higher the zirconia percentage in the silane solution, the greater the amount of ZrO_2 agglomerates deposited on the substrate (XRF) and the thicker the coating formed. Thickness measured with opto-digital microscope present similar values than the estimation with scratch. In Figure 4, images taken with the microscope are shown.

Table 2. Analysis of the composition and estimated thickness of the coatings for the different ZrO_2 percentages by XRF and scratch and roughness measurements, respectively.

Coating	% Si	% Zr	Coating Thickness (μm) (Scratch)	Coating Thickness (μm) (Opto-Digital Microscope)
Pristine steel	0.33 ± 0.02	<0.0001	–	–
0 wt.% ZrO_2	14.89 ± 3.08	<0.0001	–	–
1 wt.% ZrO_2	21.54 ± 1.26	0.03 ± 0.00	0.8 ± 0.10	1.0 ± 0.10
2.5 wt.% ZrO_2	18.48 ± 1.17	0.14 ± 0.02	1.2 ± 0.53	1.2 ± 0.10
5 wt.% ZrO_2	18.86 ± 1.57	0.24 ± 0.04	2.4 ± 0.06	2.3 ± 0.17

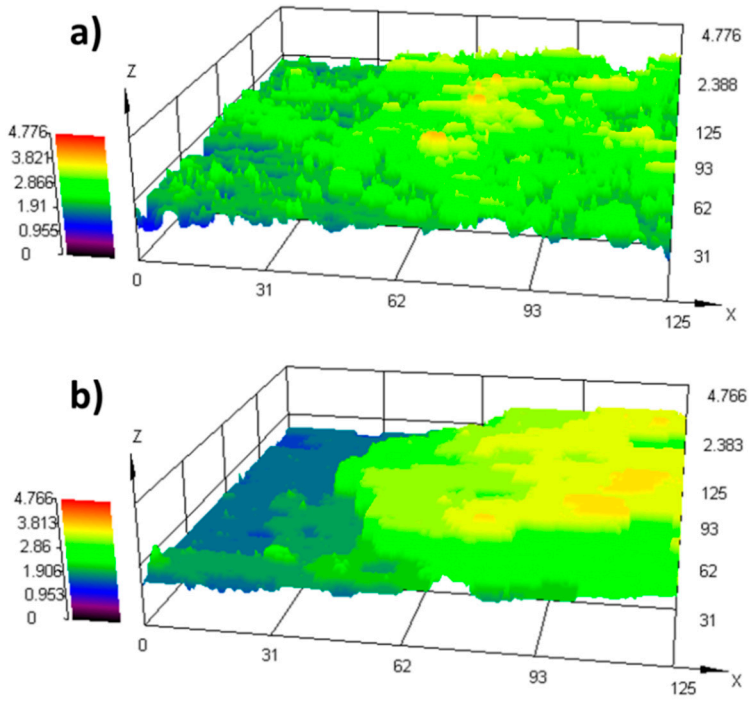

Figure 4. *Cont.*

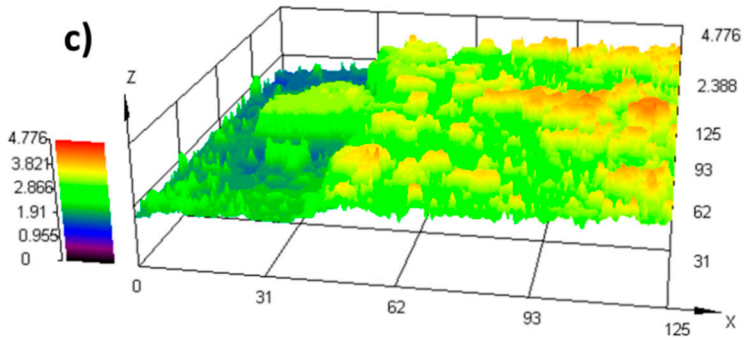

Figure 4. Images of coatings with (**a**) 1 wt.%, (**b**) 2.5 wt.%, and (**c**) 5 wt.% ZrO_2.

Figure 5 shows the FTIR spectra for the different coatings. Peaks at 3327 cm^{-1} correspond to freely vibrating OH groups, hydrogen bonded OH groups or OH groups associated to SiOH, ZrOH, and ZrH bonds [33,34,36,40]. Its presence in the coating can be related to OH groups of solvents or formed in hydrolysis and condensation reactions of silanes as subproduct (H_2O) [34]. Band at 2972 cm^{-1} is related to vibration bands C–H of alkoxy groups or solvent (occluded ethanol). Si–CH_3 bond is assigned to the peak at 1277 and 781 cm^{-1} [6,38], being directly related to MTS silane. Bands between 1160 and 1050 cm^{-1} correspond to the condensation species (Si–O–Si) [33,41] by reaction between silanol groups when the coating is curing into the oven at 110 °C. C–O bands due to ethanol can be overlapped under this broad band of siloxane groups. Finally, peaks at 910 cm^{-1} are related to silanol groups (Si–OH) [6]. Differences among spectra as a function of amount of ZrO_2 have not been found.

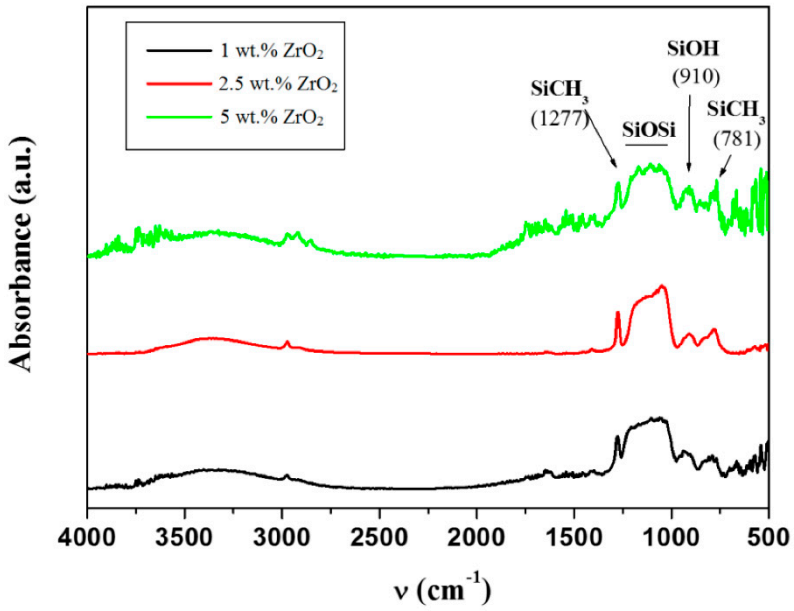

Figure 5. FTIR spectra of silane–ZrO_2 coatings.

Morphological differences among surface coatings are clearly observed in Figure 6. Figure 6a,c,e shows that the amount of ZrO_2 agglomerates observed on the surface increases with the ZrO_2 percentage added into silane solution, as it was observed by XRF as well. Besides, different sizes of agglomerates are distributed on the whole surface. The average particle size estimated from these SEM images is around 2 μm, coinciding with DLS results (Figure 3). The images at higher magnifications (Figure 6b,d,f) show that these large agglomerates consist of smaller ones.

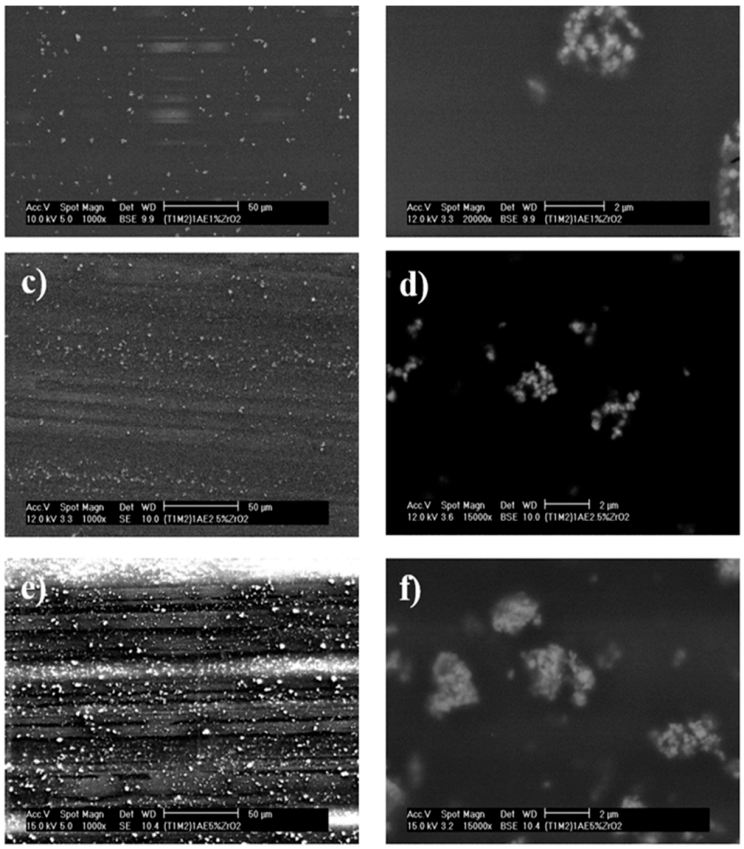

Figure 6. SEM topography images of coatings with (**a**,**b**) 1 wt.%, (**c**,**d**) 2.5 wt.%, and (**e**,**f**) 5 wt.% ZrO_2 at different magnifications.

Hydrophobic properties of these coatings were evaluated measuring water contact angles. Results are shown in Figure 7. All coatings exhibit lower wettability than pristine steel. Fei et al. [42] assure that presence of methyl groups from MTS decrease the surface energy of the surface. Previous studies using different silanes (acrylic-silane [6] and alkyl-silane [20]) show a more hydrophobic surface when silane coatings have non-polar groups (siloxane and alkyl groups). Such as it was observed by FTIR, siloxane groups are found on the coated surface (Figure 5), which are responsible of this raise of hydrophobic properties along with Si–CH_3 groups (from MTS silane). The most important increase of water contact angles is observed for the coating without particles. Adding zirconia nanoparticles decreases contact angles respect to silane coating (0 wt.% ZrO_2), between 10° and 20°. This decrease is higher for the polar liquids. This can be explained due to the polar character that ZrO_2 agglomerates provide to the surface. Differences among the three ZrO_2–silane coatings are not significant as shown in Figure 7.

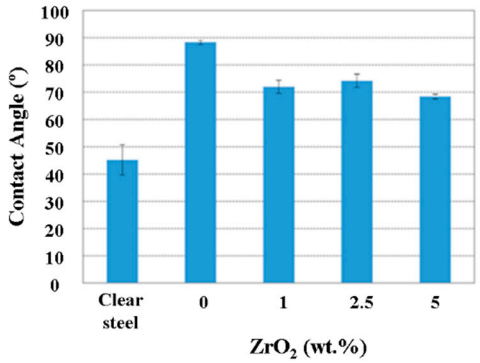

Figure 7. Contact angle of coatings with different liquids as a function of zirconia percentage added.

Aesthetical aspects of the coated plates are studied using color and specular gloss measurements. Color coordinates (L^*, a^* and b^*) and color difference to uncoated steel (ΔE) are shown in the Table 3. ΔE is calculated from the differences of its component and it informs about the significance of color change. In general terms, ZrO_2–silane coating promotes a slight loss of lightness (L^*). This loss of lightness is due to the opacity provided by ZrO_2 agglomerates. A similar tendency was already observed in previous reports for silane–SiO_2 coatings [20]. However, a^* and b^* coordinates do not display a clear trend, and the changes are not meaningful. For all coated surfaces, colorimetric differences (ΔE) are lower than 10. It informs that the change of color related to clear steel is small. This value increases when silane and nanoparticles are together on the surfaces, as it was observed in previous researches [20].

Table 3. Colorimetric parameter (L^*, a^*, b^*, and ΔE) as function of ZrO_2 percentage.

Coating	L^*	a^*	b^*	ΔE
Clear steel	68.66	0.37	4.6	–
Silane	67.44	0.40	4.33	1.24
Silane + 1 wt.% ZrO_2	65.41	0.31	3.97	3.31
Silane + 2.5 wt.% ZrO_2	64.61	0.40	4.13	4.08
Silane + 5 wt.% ZrO_2	65.78	0.51	4.26	2.90

Significant specular gloss changes (Figure 8) are observed for the silane coating, increasing more than 60% respect to clear steel, from 54 to 89 GU. However, specular gloss changes are not meaningful for silane–ZrO_2 coatings with 1 wt.% and 2.5 wt.% of nanoparticles regard to clear steel; being more noticeable for the coatings with 5 wt.% ZrO_2 (values around 30 GU are measured). However, these changes are not visible, a slight opacity can be observed only with different tilts of the plates. In conclusion, the effect of the nanoparticles on gloss is adequate for the in-service conditions, according to the architects and designers requirements.

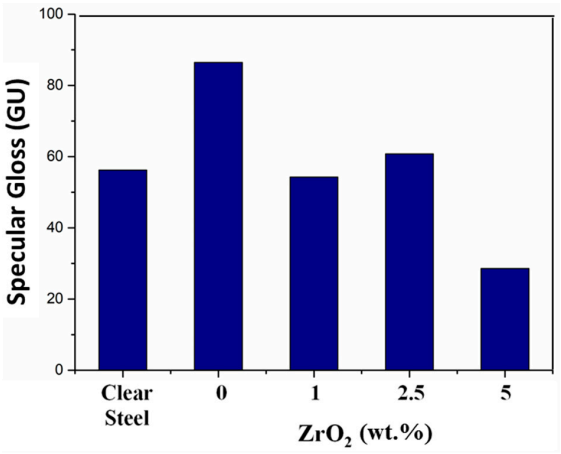

Figure 8. Variation of gloss as a function of the percentage of zirconia.

The silane coating (0 wt.% ZrO_2) and the uncoated stainless steel have the highest friction coefficients (Figure 9), 0.39 and 0.36 respectively. Moreover, it remains almost constant during the test, being changes at the beginning of the test related to the formation of wear track and wearing of steel or silane. The friction coefficient for the silane coated plate is higher than this coefficient for stainless steel, possibly due to the sticking of the coating on the pin. Previous studies about the wear resistance of silane coatings found that the presence of SiOSi groups could be related to the tribological characteristics of the coatings, taking place at lower friction coefficients and higher wear resistances [43,44]. The infrared studied shown before (Figure 5) confirms the presence of siloxane groups.

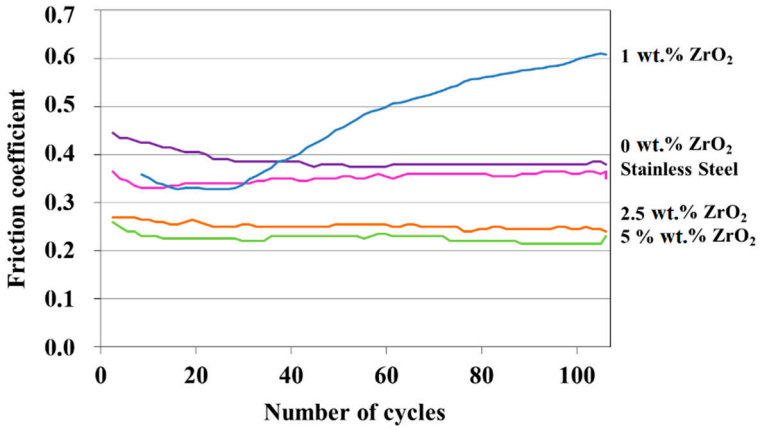

Figure 9. Friction coefficients of each surface obtained during wear test, as a function of number of cycles.

The presence of zirconia reduces friction coefficient respect to the silane coating without ZrO_2 and the uncoated surface, reaching 0.23 for coatings with 5 wt.% of ZrO_2. The higher percentage of ZrO_2 promotes the lower friction coefficient, possibly related not only to ZrO_2 amount but to presence of agglomerates (as XRF and SEM have shown), being able to stand wear. A similar conclusion was drawn by Banerjee et al. [11] for fluorosilane coatings with colloidal silica nanoparticles, showing that increasing the concentration of added silica to the sol-gel matrix led to a harder and more wear-resistant coating on the surface [45].

It is observed that the friction coefficient of coating with 1 wt.% of nanoparticles ascends after a determined number of cycles. It indicates that the coating is worn down after 28 cycles [46] and the zirconia particles are stripped off and they could act as a third body, incrementing the friction coefficient. Coatings with 2.5 wt.% and 5 wt.% of ZrO_2 do not worn after 100 cycles with 5 N of load. For this reason, another assay was carried out for these coatings.

The comparison of the two coatings with 10 N of load is shown in Figure 10. The friction coefficient of the coating with 2.5 wt.% of ZrO_2 shows an important increment after 1610 cycles with 10 N of load. It means that the coating is worn down in this moment. Coating with 5 wt.% ZrO_2 is not worn down significantly until the 3340th cycle. After this number of cycles, an increase in friction coefficient takes place, indicating that the coating is disappearing. Hence coating with 5 wt.% of ZrO_2 nanoparticles shows the highest values of wear strength.

The coating without nanoparticles does not present the increase in friction coefficient when it wears down. This is due to the lack of the third body effect when nanoparticles are not present in the coating.

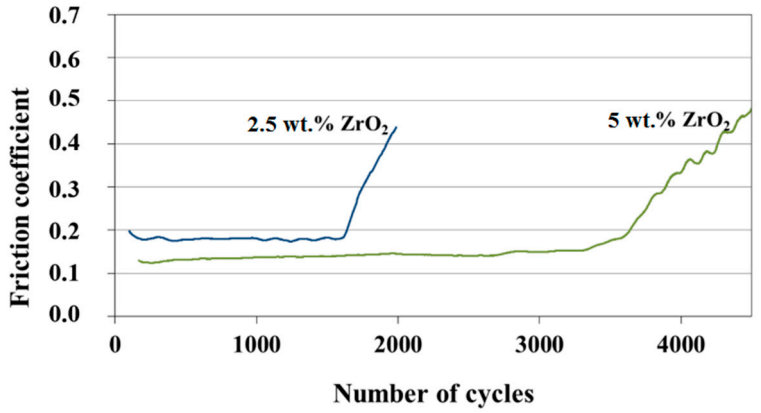

Figure 10. Friction coefficient for coatings with 2.5 wt.% and 5 wt.% of ZrO_2 with 10 N of load.

Table 4 summarizes these results. The friction coefficient when coatings are not worn down decreases when the percentage of ZrO_2 increases. It indicates that adding ZrO_2 makes the coatings harder. On the other hand, wear resistance clearly increases when the content of nanoparticles increases.

Table 4. Friction coefficient and number cycles to wear down for the coatings.

Coating	Initial Friction Coefficient	No. Cycles to Wear Down
Silane	0.38	<25 (5 N)
Silane + 1 wt.% ZrO_2	0.35	35 (5 N)
Silane + 2.5 wt.% ZrO_2	0.25	1610 (10 N)
Silane + 5 wt.% ZrO_2	0.23	3340 (10 N)

4. Conclusions

The austenitic stainless steel is successfully coated by a silane-based solution with zirconia nanoparticles. It is proved by FTIR, where the bands corresponding to silanes and zirconia were observed, and XRF, which shows an increasing percentage of zirconia. By DLS and SEM, it is observed that the nanoparticles clump to the larger aggregates in both, solutions and coatings.

The contact angle drastically increases with all the coatings, which means that wettability of surfaces decreases, protecting the surface from water and its effects, such as corrosion.

Related to aesthetical appearance, results show that gloss and color do not change significantly with the addition of a small percentage of nanoparticles (1 wt.% and 2.5 wt.%). However, for higher concentration (5 wt.%), gloss decreases drastically, although it is not appreciated with the naked eye. Therefore, it is possible to conclude that coatings with zirconia are optically transparent.

In terms of tribological properties, the friction coefficient of the coatings decreases with the addition of nanoparticles. It is also observed that coatings with a high percentage of nanoparticles stand more wear cycles.

In conclusion, coatings on stainless steel which combine wetting, tribological, and aesthetical properties were developed.

Author Contributions: Conceptualization, M.P. and J.A.; Methodology, M.P. and S.L.d.A.; Validation, J.A. and M.A.M.; Formal Analysis, M.P.; Investigation, S.L.d.A.; Data Curation, S.L.d.A.; Writing–Original Draft Preparation, M.P. and S.L.d.A.; Writing–Review and Editing, J.A. and M.A.M.; Supervision, J.A. and M.A.M.; Project Administration, M.A.M.; Funding Acquisition, M.A.M.

Funding: This research received funding from the SUDOE project SOE1/P1/E307.

Acknowledgments: The authors would like to thank to the Advanced Materials and Nanotechnology group (Mechanical Engineering Department, Universidad Pontifica Comillas-ICAI).

Conflicts of Interest: The authors declare no conflict of interest.

References

1. Pathak, S.S.; Khanna, A.S. Sol-gel nanocoatings for corrosion protection. In *Corrosion Protection and Control Using Nanomaterials*, 1st ed.; Saji, V.S., Cook, R., Eds.; Woodhead Publishing: Cambridge, UK, 2012; pp. 304–329.
2. Montoya, P.; Martins, C.R.; de Melo, H.G.; Aoki, I.V.; Jaramillo, F.; Calderón, J.A. Synthesis of polypyrrole-magnetite/silane coatings on steel and assessment of anticorrosive properties. *Electrochim. Acta* **2014**, *124*, 100–108. [CrossRef]
3. Córdoba, L.C.; Montemor, M.F.; Coradin, T. Silane/TiO_2 coating to control the corrosion rate of magnesium alloys in simulated body fluid. *Corros. Sci.* **2016**, *104*, 152–161. [CrossRef]
4. Ramezani, M.; Vaezi, M.R.; Kazemzadeh, A. Preparation of silane-functionalized silica films via two-step dip coating sol-gel and evaluation of their superhydrophobic properties. *Appl. Surf. Sci.* **2014**, *317*, 147–153. [CrossRef]
5. Ma, M.; Hill, R.M. Superhydrophobic surfaces. *Curr. Opin. Colloid Interface Sci.* **2006**, *11*, 193–202. [CrossRef]

6. Pantoja, M.; Abenojar, J.; Martínez, M.A.; Velasco, F. Silane pretreatment of electrogalvanized steels: Effect on adhesive properties. *Int. J. Adhes. Adhes.* **2016**, *65*, 54–62. [CrossRef]
7. Calabrese, L.; Bonaccorsi, L.; Caprì, A.; Proverbio, E. Adhesion aspects of hydrophobic silane zeolite coatings for corrosion protection of aluminium substrate. *Prog. Org. Coat.* **2014**, *77*, 1341–1350. [CrossRef]
8. Cheng, X.W.; Liang, C.X.; Guan, J.P.; Yang, X.H.; Tang, R.C. Flame retardant and hydrophobic properties of novel sol-gel derived phytic acid/silica hybrid organic–inorganic coatings for silk fabric. *Appl. Surf. Sci.* **2018**, *427*, 69–80. [CrossRef]
9. Suegama, P.H.; Recco, A.A.C.; Tschiptschin, A.P.; Aoki, I.V. Influence of silica nanoparticles added to an organosilane film on carbon steel electrochemical and tribological behavior. *Prog. Org. Coat.* **2007**, *60*, 90–98. [CrossRef]
10. Zhang, W.; Liu, W.; Wang, C. Characterization and tribological investigation of sol-gel Al_2O_3 and doped Al_2O_3 films. *J. Eur. Ceram. Soc.* **2002**, *22*, 2869–2876. [CrossRef]
11. Piwonski, I.; Soliwoda, K. The effect of ceramic nanoparticles on tribological properties of alumina sol-gel thin coatings. *Ceram. Int.* **2010**, *36*, 47–54. [CrossRef]
12. Zhi, Y.; Sun, X.; Li, N.; Yuan, S.; Wang, Z.; Jin, L.; Hang, J.; Shi, L. UV curable organic–inorganic hybrid coatings on microporous polyethylene separator for enhancing mechanical and electrochemical performance. *Appl. Surf. Sci.* **2018**, *743*, 756–762. [CrossRef]
13. Banerjee, D.A.; Kessman, A.J.; Cairns, D.R.; Sierros, K.A. Tribology of silica nanoparticle-reinforced, hydrophobic sol-gel composite coatings. *Surf. Coat. Technol.* **2014**, *260*, 214–219. [CrossRef]
14. Behzadnasab, M.; Mirabedini, S.M.; Kabiri, K.; Jamali, S. Corrosion performance of epoxy coatings containing silane treated ZrO_2 nanoparticles on mild steel in 3.5% NaCl solution. *Corros. Sci.* **2011**, *53*, 89–98. [CrossRef]
15. Montemor, M.F.; Trabelsi, W.; Lamaka, S.V.; Yasakau, K.A.; Zheludkevich, M.L.; Bastos, A.C.; Ferreira, M.G.S. The synergistic combination of bis-silane and $CeO_2{\cdot}ZrO_2$ nanoparticles on the electrochemical behaviour of galvanised steel in NaCl solutions. *Electrochim. Acta* **2008**, *53*, 5913–5922. [CrossRef]
16. Gusmano, G.; Montesperelli, G.; Rapone, M.; Padeletti, G.; Cusmà, A.; Kaciulis, S.; Mezzi, A.; Di Maggio, R. Zirconia primers for corrosion resistant coatings. *Surf. Coat. Technol.* **2007**, *201*, 5822–5828. [CrossRef]
17. Zhu, R.; Zhang, J.; Chang, C.; Gao, S.; Ni, N. Effect of silane and zirconia on the thermal property of cathodic electrophoretic coating on AZ31 magnesium alloy. *J. Magnes. Alloy.* **2013**, *1*, 235–241. [CrossRef]
18. Mirabedini, S.M.; Behzadnasab, M.; Kabiri, K. Effect of various combinations of zirconia and organoclay nanoparticles on mechanical and thermal properties of an epoxy nanocomposite coating. *Compos. Part A Appl. Sci. Manuf.* **2012**, *43*, 2095–2106. [CrossRef]
19. Liu, X.; Yang, Q.; Li, Z.; Yuan, W.; Zhen, Y.; Cui, Z.; Yang, X.; Yeung, K.W.K.; Wu, S. A combined coating strategy based on atomic layer deposition for enhancement of corrosion resistance of AZ31 magnesium alloy. *Appl. Surf. Sci.* **2018**, *434*, 1101–1111. [CrossRef]
20. Kumar, P.; Oka, M.; Ikenchi, K.; Shimizu, K.; Yamamuro, T.; Okumura, H.; Kotoura, Y. Low wear rate of UHMWPE against zirconia ceramic (Y-PSZ) in comparison to alumina ceramic and SUS 316L alloy. *J. Biomed. Mater. Res.* **1991**, *25*, 813–828. [CrossRef] [PubMed]
21. Kurahatti, R.V.; Surendranathan, A.O.; Srivastava, S.; Singh, N.; Ramesh Kumar, A.V.; Suresha, B. Role of zirconia filler on friction and dry sliding wear behaviour of bismaleimide nanocomposites. *Mater. Des.* **2011**, *32*, 2644–2649. [CrossRef]
22. Yen, S.K.; Guo, M.J.; Zan, H.Z. Characterization of electrolytic ZrO_2 coating on CoCrMo implant alloys of hip prosthesis. *Biomaterials* **2001**, *22*, 125–133. [CrossRef]
23. Pantoja, M.; Abenojar, J.; Martinez, M.A. Influence of the type of solvent on the development of superhydrophobicity from silane-based solution containing nanoparticles. *Appl. Surf. Sci.* **2017**, *397*, 87–94. [CrossRef]
24. Gonnet, J. Colour effects of co-pigmentation of anthocyanins revisited—2. A colorimetric look at the solucions of cyanin co-pigmented by rutin using the CIELAB scale. *Food Chem.* **1999**, *66*, 387–394. [CrossRef]
25. Franceschi, E.; Letardi, P.; Luciano, G. Colour measurements on patinas and coatings system for outdoor bronze monuments. *J. Cult. Herit.* **2006**, *7*, 166–170. [CrossRef]
26. Berry, J.D.; Neeson, M.J.; Dagastine, R.R.; Chan, D.Y.C.; Tabor, R.F. Measurement of surface and interfacial tension using pendant drop tensiometry. *J. Colloid Interface Sci.* **2015**, *454*, 226–237. [CrossRef] [PubMed]
27. Lewis, J.A. Colloidal processing of ceramics. *J. Am. Ceram. Soc.* **2000**, *83*, 2341–2359. [CrossRef]

28. Tang, F.; Huang, X.; Zhang, Y.Z.; Guo, J. Effect of dispersants on surface chemical properties of nano-zirconia supensions. *Ceram. Int.* **2000**, *26*, 93–97. [CrossRef]
29. Dos Santos, V.; da Silveira, N.P.; Bergmann, C.P. In-situ evaluation of particle size distribution of ZrO_2-nanoparticles obtained by sol-gel. *Powder Technol.* **2014**, *267*, 392–397. [CrossRef]
30. Puomi, P.; Fagerholm, H.M. Charaterization of hot-dip galvanized (HDG) steel treated with UPS, VS and tetrasulfide. *J. Adhes. Sci. Technol.* **2001**, *15*, 509–533. [CrossRef]
31. Zhou, Z.H.; Zhang, Q.; Wang, H.Z.; Xu, Z.C.; Zhang, L.; Liu, D.D.; Zhang, L. Wettability of a PTFE surface by aqueous solutions of zwitterionic surfactants: Effect of molecular structure. *Colloids Surf. A* **2016**, *489*, 370–377. [CrossRef]
32. Anderson, D.R. Infra-red, Raman and ultraviolet spectroscopy. In *Analysis of Silicones*; Smith, A.L., Ed.; Wiley Interscience: New York, NY, USA, 1974; pp. 247–286.
33. Pantoja, M.; Encinas, N.; Abenojar, J.; Martínez, M.A. Effect of tetraethoxysilane coating on the improvement of plasma treated polypropylene adhesion. *Appl. Surf. Sci.* **2013**, *280*, 850–857. [CrossRef]
34. Nadargi, D.Y.; Latthe, S.S.; Venkateswara, A. Effect of post-treatment (gel aging) on the properties of methyltrimethoxysilane based silica aerogels prepared by two-step sol-gel process. *J. Sol-Gel Sci. Technol.* **2009**, *49*, 53–59. [CrossRef]
35. Socrates, G. *Infrared and Raman Characteristic Group Frequencies*, 3rd ed.; John Willey & Sons: Chichester, UK, 2001.
36. Department of Chemistry and Biochemistry, University of Colorado at Boulder. Organic Chemistry al CU Boulder. Available online: http://orgchem.colorado.edu/Spectroscopy/irtutor/alcoholsir.html (accessed on 5 April 2016).
37. Pantoja, M.; Velasco, F.; Broekema, D.; Abenojar, J.; del Real, J.C. The influence of pH on the hydrolysis process of γ-Methacryloxypropyltrimethoxysilane, analyzed by FT-IR, and the silanization of electrogalvanized steel. *J. Adhes. Sci. Technol.* **2010**, *24*, 1131–1143. [CrossRef]
38. Onishi, T.; Abe, H.; Maruya, K.; Domen, K. I.r. spectra of hydrogen absorbed on ZrO_2. *J. Chem. Soc. Chem. Commun.* **1985**, 617–618. [CrossRef]
39. Onishi, T. IR spectroscopic studies on surface reactions. In *Dynamic Processes on Solid Surfaces*, 1st ed.; Tamaru, K., Ed.; Springer: New York, NY, USA, 1993; pp. 237–257.
40. Phanasgaonkar, A.; Raja, V.S. Influence of curing temperatura, silica nanoparticles- and cerium on surface morphology and corrosion behavior of hybrid silane coatings on mild steel. *Surf. Coat. Technol.* **2009**, *203*, 2260–2271. [CrossRef]
41. Kapoor, P.; Mhaske, S.T.; Joshi, K. Modification and characterisation of pre-hydrolysed silanes by acrylate utilizing sol–gel process. *Prog. Org. Coat.* **2016**, *94*, 124–130. [CrossRef]
42. Fei, T.; Chen, H.; Lin, J. Transparent superhydrophobic films possessing high thermal stability and improved moisture resistance from the deposition of MTMS-based aerogels. *Colloids Surf. A* **2014**, *443*, 255–264. [CrossRef]
43. Múgica, R.; Alba, F.; Sainz, E.; Pantoja, M. Hydrophobicity attainment and wear resistance enhancement on glass substrates by atmospheric plasma-polymerization of mixtures of an aminosilane and a fluorocarbon. *Appl. Surf. Sci.* **2015**, *347*, 325–335. [CrossRef]
44. Masuko, M.; Miyamoto, H.; Suzuki, A. Tribological characteristics of self-assembled monolayer with siloxane bonding to Si surface. *Tribol. Int.* **2007**, *40*, 1587–1596. [CrossRef]
45. Kahn, H.; Ernst, F.; Heuer, A.H. Increasing the coefficient of sliding friction of NiCr at low loads by interstitial surface hardening. *Wear* **2016**, *346–347*, 1–5. [CrossRef]
46. Ou, Y.X.; Lin, J.; Tong, S.; Che, H.L.; Sproul, W.D.; Lei, M.K. Wear and corrosion resistance of CrN/TiN superlattice coatings deposited by a combined deep oscillation magnetron sputtering and pulsed dc magnetron sputtering. *Appl. Surf. Sci.* **2015**, *351*, 332–343. [CrossRef]